On the sequence of deformable mirrors in MCAO: findings from an on-sky, closed-loop experiment

Schmidt, Dirk, Gorceix, Nicolas, Goode, Philip

Dirk Schmidt, Nicolas Gorceix, Philip Goode, "On the sequence of deformable mirrors in MCAO: findings from an on-sky, closed-loop experiment," Proc. SPIE 11448, Adaptive Optics Systems VII, 1144842 (14 December 2020); doi: 10.1117/12.2563376

SPIE.

Event: SPIE Astronomical Telescopes + Instrumentation, 2020, Online Only

On the sequence of deformable mirrors in MCAO: findings from an on-sky, closed-loop experiment

Dirk Schmidt[a], Nicolas Gorceix[b], and Philip Goode[b]

[a]National Solar Observatory, 3665 Discovery Drive, Boulder, CO 80303, USA
[b]New Jersey Inst. of Tech., Big Bear Solar Obs., 40386 N Shore Ln, Big Bear City, CA 92314, USA

ABSTRACT

We performed an on-sky MCAO experiment using 4 deformable mirrors (DMs) to analyze the relevance of their sequence to the residual wavefront error. Two DMs were conjugate to 4 and 8 km. The other two DMs were placed in pupil images upstream and downstream of the 4-km and 8-km mirrors. At any time, both high altitude DMs were active but only one pupil DM was active while the other one stayed flat. Firstly, we found that the MCAO control loops using either pupil DM were stable and robust. Dynamic misregistration, which was present for the first pupil DM, was not an immediate problem for the controller. We did not notice an apparent difference when repeatedly switching between the pupil DMs during the operation. A closer analysis of the contrast in the corrected images and AO telemetry indicates an advantage when the pupil correction was applied with the DM that was downstream of the high-altitude DMs. This finding is consistent in several data recorded at different days. The difference, however, is small. A more detailed analysis is probably needed to rule out error sources potentially not considered herein to draw a final conclusion on the optimal sequence of DMs in MCAO and its practical relevance.

Keywords: multi-conjugate adaptive optics, sequence of deformable mirrors, dynamic misregistration, Clear

1. INTRODUCTION

In multi-conjugate adaptive optics (MCAO), a sequence of multiple deformable mirrors (DMs) is used in a telescope to correct the image for atmospheric turbulence.[1,2] Each mirror is located at a position that corresponds to ("is conjugate to") a different distance in front of the telescope on its optical axis, therefore correcting turbulence occurring at layers of different altitudes in the atmosphere. Since multiple deformable mirrors are used sequentially in MCAO, the question may arise in what sequence should those mirrors be placed in the telescope for best correction. So far, this question has only been addressed theoretically. In 1998, Hardy [3, page 53 ff.] wrote *"Multiple layers must be corrected in an optical sequence determined by their distance from the telescope, the nearest layers being corrected first."*, arguing that this way, the deformable mirrors and the turbulent layers form a set of nested systems in which each level of nesting (from lower to higher altitudes) is free of wavefront aberrations. In 2000, Flicker[4] performed a quantitative theoretical analysis of a setup with two DMs and concluded *"The reduction in Strehl ratio can be as large as 10–15%, depending strongly on wavelength, turbulence profile, and zenith angle."* if the high-altitude DM comes first and *"Hence MCAO systems should address the issue of relay optics in the conjugate range, in particular if the systems are designed to operate at visible wavelengths."* Farley et al.[5] drew a similar conclusion more recently: *"This has the potential to reduce the achievable Strehl ratio by as much as 15% on NFIRAOS at 500 nm."* While these authors indicated some advantage when correcting the lower layers first, their pictures concentrated on the manipulation of the phase and did not include any realistic wavefront sensor or AO control loop.

In a telescope with MCAO, any DM not conjugate to the pupil distorts the subsequent image of the pupil plane when it changes its shape. If the ground layer is corrected first, with a DM that is located in a pupil image before a high-altitudes DM as advised by Hardy, a subsequent wavefront sensor suffers from *dynamic misregistration*.[6] We showed earlier that dynamic misregistration makes an MCAO system non-linear in the sense that the response on the wavefront sensor becomes a function of the product of actuator motion and that if the distortion becomes too large, the registration would ultimately be destroyed.[7] While one could expect systems with small actuator pitches and subapertures (projected to the primary mirror) to be more susceptible to suffer from dynamic misregistration, the practical relevance and the additional error introduced

Send correspondence to Dirk Schmidt, e-mail: dschmidt@nso.edu

Adaptive Optics Systems VII, edited by Laura Schreiber, Dirk Schmidt, Elise Vernet, Proc. of SPIE
Vol. 11448, 1144842 · © 2020 SPIE · CCC code: 0277-786X/20/$21 · doi: 10.1117/12.2563376

by this effect is not well understood. The commonly used end-to-end simulation tools Blur/KAOS,[8] CAOS,[9] COMPASS,[10] DASP,[11] MAOS,[12] Octopus,[13] OOMAO,[14] Soapy,[15] and Yao[16] do not model the effects relevant in this context. At this conference, a simulation tool is presented that could potentially be used to study the DM sequence in a more complete theoretical picture.[17]

Since the early 2000s, on-sky MCAO control loops have been closed at eight astronomical telescopes. In the solar telescopes VTT,[18] DST,[19,20] Gregor,[21,22] and NVST,[23] as well as in the LBT's LINC-NIRVANA[24] with its adaptive secondary mirror, the turbulence near the ground was corrected before the turbulence in higher altitudes. In MAD[25] on the VLT and in GeMS[26,27] at the Gemini South Observatory, the high altitude turbulence was corrected first.

Our MCAO pathfinder Clear on the Goode Solar Telescope includes two pupil images that are suitable for a deformable mirror—one pupil being located before, one behind two high-altitude DMs.[28,29] We have used a DM in either pupil image with a multi-directional wavefront sensor with 8.8-cm subapertures behind all DMs successfully since 2016. The control loop appeared to perform equally well in either configuration. A quantitative comparison under equal conditions, however, could not be made because we had only 3 DMs, and we had to move one DM from one pupil to the other. An effort that takes several hours. To make that quantitative comparison, we upgraded Clear temporarily in 2019 with a fourth DM and occupied both pupil images with DMs.

2. EXPERIMENTAL SETUP OF CLEAR WITH FOUR DEFORMABLE MIRRORS

Clear is the MCAO system on the 1.6-m off-axis Goode Solar Telescope at the Big Bear Solar Observatory in Southern California. Clear has served as an experimental pathfinder since 2013. Since 2016, Clear delivers a high-order corrected field of view of about 35 arcsec.[30] Since 2020, Clear can feed the spectro-polarimetric instrument suite at the Goode Solar Telescope and has been used for science observations including flare patrols. Clear has been designed to provide at least six different configurations to test various approaches and sequences of wavefront sensing and correction with three deformable mirrors. A list is available in reference 29. In September of 2019, we combined configurations 5 and 6 into a configuration with four DMs as shown in Figure 1. In this configuration, we had two DMs that are conjugate to the pupil of the telescope. One pupil is before and one after the DMs in 4 and 8 km. The temporarily added fourth DMs is the old 97-actuator Xinetics mirror of the AO system of the previous 60-cm telescope at Big Bear. We used this mirror as the DM in 8 km. The other three mirrors models are Clear's normal 357-actuator mirrors by Xinetics. The pupil on $\mathrm{DM}_{\mathrm{pupil\ 1}}$ is 100 mm large, and 90 mm on $\mathrm{DM}_{\mathrm{pupil\ 2}}$. That is, the actuator pitch projected onto the primary mirror was 8 cm on $\mathrm{DM}_{\mathrm{pupil\ 1}}$, and 8.8 cm on $\mathrm{DM}_{\mathrm{pupil\ 2}}$. The projected actuator pitches in $\mathrm{DM}_{4\ \mathrm{km}}$ and $\mathrm{DM}_{8\ \mathrm{km}}$ were approximately 19 and 34 cm, respectively.

The multi-directional correlating Shack-Hartmann wavefront sensor (MD-WFS) for the MCAO control loop was unaltered from the Clear standard setup: The subaperture size is 8.8 cm matching the actuator pitch on $\mathrm{DM}_{\mathrm{pupil\ 2}}$. The outer ring of subapertures that are close to the pupil edge are dismissed in the wavefront reconstruction. We do this because the *dynamic pupil distortion* in MCAO randomly and continuously changes the illumination and degrades the measurement in those subapertures. In total, we use 208 subapertures (16 across) and 3×3 guide-regions over a field of view of about 35×35 arcsec.

We used two cameras in the MCAO corrected image plane recording images at different wavelengths. There is a small pupil image after the beam splitter for the MD-WFS. We stopped down this pupil to an effective aperture size of about 1.42 meters which corresponds to diameter that is used for the wavefront sensing. This way, we eliminate the uncorrected annulus in the wavefront for these cameras. This stop also removes the intensity fluctuations that would otherwise be present in the MCAO corrected image plane.[31] A PCO 2000 camera recorded the image in titanium oxide line at about 706 nm, and a PCO Panda 4.2 bi recorded images in the Hα or Calcium II K lines at about 656 and 393 nm, respectively.

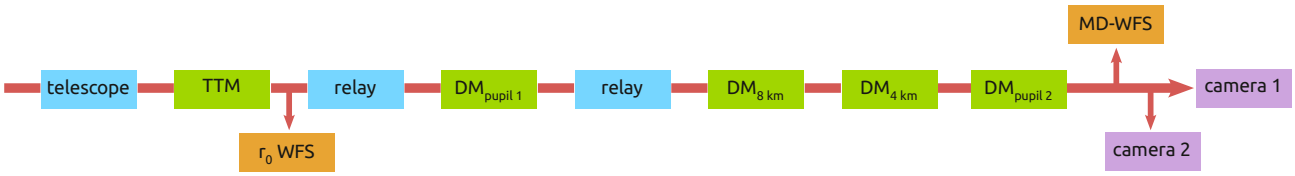

Figure 1: Schematic of the sequence of elements that the light passes in the telescope. (Not all optics included)

A second multi-directional wavefront sensor located after the tip-tilt mirror (TTM) but before the first deformable mirror was used to estimate the Fried parameter r_0 from the analysis of differential image motion[32] in 13 directions over 85×85 arcsec with a subaperture size of 12 cm. This wavefront sensor recorded data at 500 fps and had no connection to the MCAO control loop. It is only used herein for post-facto analysis of the Fried parameter.

In order to compare the MCAO correction using each pupil DM, we had the control loop running at 1500 Hz and switched automatically between the pupil DMs about every 2 seconds. The switching was done by replacing the control matrix between loop cycles with no interruption. The exact same sets of Karhunen-Loève modes were used to reconstruct the wavefront in the pupil for both DMs and projected accordingly onto the DMs accounting for their particular actuator spacing. The set of modes for the high-altitude reconstruction was also fixed. The leaky integrator in the controller ramped down the figure of a pupil DM after it was switched off over some loop cycles. Both cameras recorded images at their maximum frame rate for about 20 seconds and stored high-resolution time stamps for every frame. We also recorded all MCAO control status data for each loop cycle. We typically started a recording with tip-tilt-only correction and then switched on the correction with the three respective DMs. We did this to mark the images recorded in the MCAO image plane to be able to exactly synchronize the time stamps in camera frames with the MCAO telemetry for the present analysis. The cross-correlation reference image was not updated over the course of the recording in order to avoid any effect that could impact the correction such as a different signal-to-noise ratio in the reference image. As a result, the correction could gradually degrade over time regardless of the DM switching and seeing as the reference image gets older and older while the structure on the sun keeps evolving.

3. DATA ANALYSIS

3.1 Image contrast

For each camera image, we applied dark and flat field correction and then computed the RMS image contrast $\sigma(I)/\langle I\rangle$ in a 64×64 px box in the center. In order to identify the offset in the time stamps in the camera images and in the control loop data, we visually looked for the images in the bursts in which the switching from tip-tilt-only to MCAO correction occurred. This switch is easily visible. From there on, we matched the camera images with the status data of the MCAO controller based on their time stamps to reconstruct which of the two pupil DMs was active in which camera image.

In Figures 2, 3, and 4, we show the resulting image contrast for three exemplary datasets. "Pupil corrector last" means $\mathrm{DM}_{\mathrm{pupil\,2}}$ was active, and "Pupil corrector first" means $\mathrm{DM}_{\mathrm{pupil\,1}}$ was active, while the other one was at rest. The box plots show the 25th, 50th (median) and 75th percentile of the correspondingly colorized data sections. The whiskers span 99% of all data points. Outliers are not shown. "Total of all" means the analysis of all data points in which $\mathrm{DM}_{\mathrm{pupil\,1}}$ and respectively $\mathrm{DM}_{\mathrm{pupil\,2}}$ was active. (The positions of the boxes and whiskers are not exactly aligned with the time axis due to difficulties with the plotting software, but in fact are computed for the matching set of data points.) The Fried parameter r_0 was estimated using 500 frames (1 sec) from the separate wavefront sensor. The time axes in the Fried parameter and the image contrasts are only synchronized to about 1 second. The scale of r_0 in those plots was not carefully calibrated and should only be used as a relative reference.

3.2 Residual wavefront error

We used the image motions (wavefront slopes) in the MD-WFS stored by the MCAO controller to estimate the residual wavefront error in each of the 9 sensing directions for each control loop cycle. This was done post-facto with a different reconstruction matrix than in the controller as the controller directly computes the ground-layer without estimating the directional error. Figures 5, 6, and 7 show the residual errors analogous to the previous plots. The variance in the data points is relatively large and we did not find it useful to plot those more than 30000 data points individually. For this reason, we only show the boxes and whiskers for the respective data sections. Here, too, the scale of the wavefront error was not carefully calibrated and should be used as a relative reference only.

4. DISCUSSION

Firstly, we showed that the pupil correction in MCAO can be done both before and after the correction of higher altitude turbulence—even with small subapertures—similarly well. Dynamic misregistration, which was present for $\mathrm{DM}_{\mathrm{pupil\,1}}$ but not for $\mathrm{DM}_{\mathrm{pupil\,2}}$, was not an immediate problem to the control loop and its stability. With a DM in either pupil image, the control loop can run stable and smooth with no apparent difference to the operator.

A closer look at both the recorded image contrasts and the residual wavefront errors consistently reveals a statistical benefit when the pupil correction was performed with $DM_{pupil\ 2}$ rather than $DM_{pupil\ 1}$, i. e. after the high-altitude correction. The difference is small but evident and is in contradiction to the theoretical models that did not include a control loop and wavefront sensors. A possible reason for the observed better performance when the pupil was corrected last could be that the effect of dynamic misregistration adds an error that is larger than the error due to the sequence of the phase correction itself. Another possibility could be that the correction with $DM_{pupil\ 1}$ was in general slighty worse because its actuator pitch is a little bit smaller than the subapertures in the wavefront sensor.

In order to draw a final conclusion whether one sequence is better than the other, we are planning to re-run the experiment. Next time, we should also record data with pupil-correction only—switching between $DM_{pupil\ 1}$ and $DM_{pupil\ 2}$ while $DM_{4\ km}$ and $DM_{8\ km}$ remain at rest. This way we should be able to identify differences related to the different DMs, either because of the actuator spacing or because of the flatness of the DMs. We should also double-check their current flatness interferometrically. Since both pupil DMs are identical, we could also interchange them. Until we have the chance to re-do this experiment, we conclude from the presented experiment that the sequence of deformable mirrors in our real MCAO system Clear with small subapertures does not have a big impact on the image correction. While there may be various reasons to prefer one sequence over the other, the practical relevance of the sequence with regard to the wavefront error has to be analyzed in finer detail.

ACKNOWLEDGMENTS

A number of people have contributed in various form to this observing run. We would particularly like to name and thank J. Nenow, E. Norro, C. Plymate, S. Shumko, and J. Varsik (all BBSO). This research was sponsored by the U.S. National Science Foundation under the grant NSF-AST-1907364. Any opinions, findings and conclusions or recommendations expressed in this publication are those of the author(s) and do not necessarily reflect the views of the National Science Foundation. The Big Bear Solar Observatory and its Goode Solar Telescope are facilities of the New Jersey Institute of Technology.

REFERENCES

[1] Beckers, J. M., "Increasing the Size of the Isoplanatic Patch with Multiconjugate Adaptive Optics," in [*Very Large Telescopes and their Instrumentation*], *ESO conference and Workshop Proceedings* **30**, 693 (1988).

[2] Dicke, R. H., "Phase-contrast detection of telescope seeing errors and their correction," ApJ **198**, 605–615 (June 1975). doi:10.1086/153639.

[3] Hardy, J. W., [*Adaptive Optics for Astronomical Telescopes*]. ISBN 9780195090192 (July 1998).

[4] Flicker, R. C., "Sequence of phase correction in multiconjugate adaptive optics," *Optics Letters* **26**, 1743–1745 (Nov. 2001). doi:10.1364/OL.26.001743.

[5] Farley, O., Osborn, J., Morris, T., Reeves, A., and Wilson, R. W., "Deformable Mirror configuration in MCAO: is propagation a fundamental limit on visible wavelength correction?," *AO4ELT5 Proceedings* (2017). doi:10.26698/AO4ELT5.0091.

[6] Schmidt, D., Berkefeld, T., Feger, B., and Heidecke, F., "Latest achievements of the MCAO testbed for the GREGOR Solar Telescope," in [*Adaptive Optics Systems II*], *Proc. SPIE* **7736** (July 2010). doi:10.1117/12.857117.

[7] Schmidt, D., Berkefeld, T., and Heidecke, F., "The 2012 status of the MCAO testbed for the GREGOR solar telescope," in [*Adaptive Optics Systems III*], Proc. SPIE **8447**, 84473J (July 2012). doi:10.1117/12.926902.

[8] Marino, J., Carlisle, R., and Schmidt, D., "Simulation of DKIST adaptive optics system," in [*Adaptive Optics Systems V*], Proc. SPIE **9909**, 99097C–99097C–17 (2016). doi:10.1117/12.2232060.

[9] Carbillet, M. and La Camera, A., "The CAOS Problem-Solving Environment: tools for AO numerical modeling and post-AO deconvolution," *AO4ELT5 Proceedings* (2017). doi:10.26698/AO4ELT5.0059.

[10] Ferreira, F., Gratadour, D., Sevin, A., Doucet, N., Vidal, F., Deo, V., and Gendron, E., "Real-time end-to-end AO simulations at ELT scale on multiple GPUs with the COMPASS platform," in [*Adaptive Optics Systems VI*], Proc. SPIE **10703**, 1070347 (July 2018). doi:10.1117/12.2312593.

[11] Basden, A., Bharmal, N., Jenkins, D., Morris, T., Osborn, J., Jia, P., and Staykov, L., "The Durham Adaptive Optics Simulation Platform (DASP): Current status," *SoftwareX* **7** (02 2018). doi:10.1016/j.softx.2018.02.005.

[12] Wang, L. and Ellerbroek, B., "Fast End-to-End Multi-Conjugate AO Simulations Using Graphical Processing Units and the MAOS Simulation Code," in [*Proceedings of the Second AO4ELT Conference*], (2011).
[13] Le Louarn, M., Vérinaud, C., Korkiakoski, V., Hubin, N., and Marchetti, E., "Adaptive optics simulations for the European Extremely Large Telescope," in [*Advances in Adaptive Optics II*], Proc. SPIE **6272**, 627234 (June 2006). doi:10.1117/12.670187.
[14] Conan, R. and Correia, C., "Object-oriented Matlab adaptive optics toolbox," in [*Adaptive Optics Systems IV*], Proc. SPIE **9148**, 91486C (Aug. 2014). doi:10.1117/12.2054470.
[15] Reeves, A., "Soapy: an adaptive optics simulation written purely in Python for rapid concept development," in [*Adaptive Optics Systems V*], Proc. SPIE **9909**, 99097F (July 2016). doi:10.1117/12.2232438.
[16] Rigaut, F. and Van Dam, M., "Simulating Astronomical Adaptive Optics Systems Using Yao," in [*Proceedings of the Third AO4ELT Conference*], (Dec. 2013). doi:10.12839/AO4ELT3.13173.
[17] van Dam, M. A., Martin Hernando, Y., Nunez Cagigal, M., Hegwer, S. L., and Montoya, L. M., "Overcoming the effect of pupil distortion in multiconjugate adaptive optics," in [*Adaptive Optics Systems VII*], Proc. SPIE **11448**.
[18] Berkefeld, T., Soltau, D., and von der Luehe, O., "Results of the multi-conjugate adaptive optics system at the German solar telescope, Tenerife," in [*Astronomical Adaptive Optics Systems and Applications II*], Proc. SPIE **5903** (Aug. 2005). doi:10.1117/12.619132.
[19] Rimmele, T., Richards, K., Roche, J., Hegwer, S., and Tritschler, A., "Progress with solar multi-conjugate adaptive optics at NSO," in [*Advances in Adaptive Optics II*], Proc. SPIE **6272**, 627206 (June 2006). doi:10.1117/12.671603.
[20] Rimmele, T. R., Woeger, F., Marino, J., Richards, K., Hegwer, S., Berkefeld, T., Soltau, D., Schmidt, D., and Waldmann, T., "Solar multiconjugate adaptive optics at the Dunn Solar Telescope," in [*Adaptive Optics Systems II*], Proc. SPIE **7736**, 773631 (July 2010). doi:10.1117/12.857485.
[21] Berkefeld, T., Soltau, D., Schmidt, D., and von der Lühe, O., "Adaptive optics development at the German solar telescopes," *Applied Optics* **49**, G155 (Sept. 2010). doi:10.1364/AO.49.00G155.
[22] Schmidt, D., Berkefeld, T., Heidecke, F., Fischer, A., von der Lühe, O., and Soltau, D., "GREGOR MCAO looking at the Sun," in [*Adaptive Optics Systems IV*], Proc. SPIE **9148**, 91481T (July 2014). doi:10.1117/12.2055154.
[23] Zhang, L., Kong, L., Bao, H., Zhu, L., Rao, X., and Rao, C., "Preliminary result of the solar multi-conjugate adaptive optics for 1m new vacuum solar telescope," in [*Adaptive Optics Systems V*], Proc. SPIE **9909**, 99092C (July 2016). doi:10.1117/12.2231955.
[24] Herbst, T. M., Santhakumari, K. K. R., Klettke, M., Arcidiacono, C., Bergomi, M., Bertram, T., Berwein, J., Bizenberger, P., Briegel, F., Farinato, J., et al., "Commissioning multi-conjugate adaptive optics with LINC-NIRVANA on LBT," in [*Adaptive Optics Systems VI*], Proc. SPIE **10703**, 107030B (July 2018). doi:10.1117/12.2313421.
[25] Marchetti, E., Brast, R., Delabre, B., Donaldson, R., Fedrigo, E., Frank, C., Hubin, N., Kolb, J., Lizon, J.-L., Marchesi, M., Oberti, S., Reiss, R., Santos, J., Soenke, C., Tordo, S., Baruffolo, A., Bagnara, P., and CAMCAO Consortium, "On-sky Testing of the Multi-Conjugate Adaptive Optics Demonstrator," *The Messenger* **129**, 8–13 (Sept. 2007).
[26] Rigaut, F., Neichel, B., Boccas, M., d'Orgeville, C., Vidal, F., van Dam, M. A., Arriagada, G., Fesquet, V., Galvez, R. L., Gausachs, G., and 20 others, "Gemini multiconjugate adaptive optics system review - I. Design, trade-offs and integration," MNRAS **437**, 2361–2375 (Jan. 2014). doi:10.1093/mnras/stt2054.
[27] Neichel, B., Rigaut, F., Vidal, F., van Dam, M. A., Garrel, V., Carrasco, E. R., Pessev, P., Winge, C., Boccas, M., d'Orgeville, C., et al., "Gemini multiconjugate adaptive optics system review - II. Commissioning, operation and overall performance," MNRAS **440**, 1002–1019 (May 2014). doi:10.1093/mnras/stu403.
[28] Schmidt, D., Gorceix, N., Zhang, X., Marino, J., Coulter, R., Shumko, S., Goode, P., Rimmele, T., and Berkefeld, T., "The multi-conjugate adaptive optics system of the New Solar Telescope at Big Bear Solar Observatory," in [*Adaptive Optics Systems IV*], Proc. SPIE **9148**, 91482U (July 2014). doi:10.1117/12.2055146.
[29] Schmidt, D., Gorceix, N., Marino, J., Berkefeld, T., Rimmele, T., Zhang, X., Wöger, F., and Goode, P., "Progress in multi-conjugate adaptive optics at Big Bear Solar Observatory," in [*Adaptive Optics Systems V*], Proc. SPIE **9909**, 990929 (July 2016). doi:10.1117/12.2232087.
[30] Schmidt, D., Gorceix, N., Goode, P. R., Marino, J., Rimmele, T., Berkefeld, T., Wöger, F., Zhang, X., Rigaut, F., and von der Lühe, O., "Clear widens the field for observations of the Sun with multi-conjugate adaptive optics," A&A **597**, L8 (Jan. 2017). doi:10.1051/0004-6361/201629970.
[31] von der Lühe, O., "Photometric stability of multiconjugate adaptive optics," in [*Advancements in Adaptive Optics*], Proc. SPIE **5490**, 617–624 (Oct. 2004). doi:10.1117/12.553053.
[32] Sarazin, M. and Roddier, F., "The ESO differential image motion monitor," A&A **227**, 294–300 (Jan. 1990).

Figure 2: Image contrasts and seeing recorded at 21:13:39 UT, Sep 6, 2019

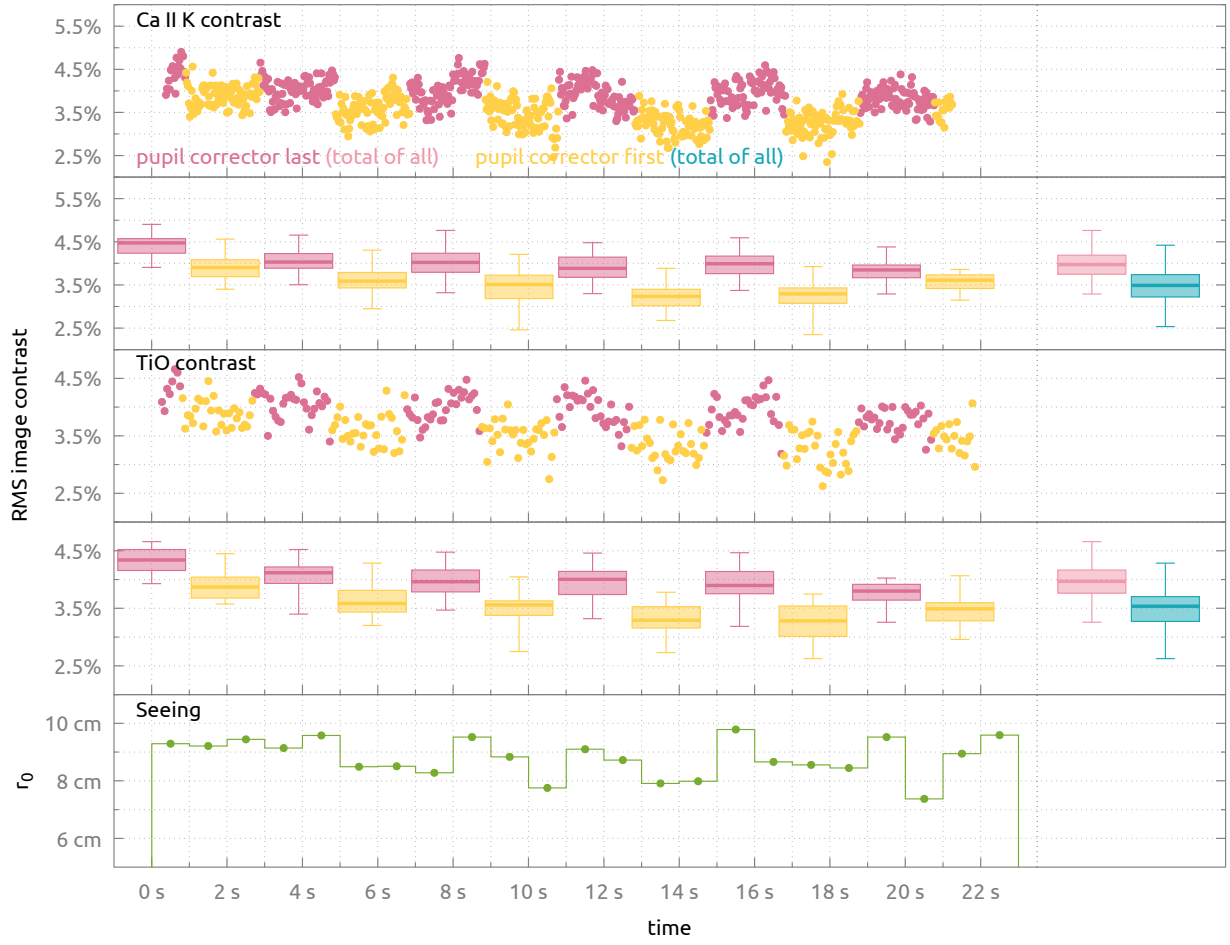

Figure 3: Image contrasts and seeing recorded at 21:18:35 UT, Sep 6, 2019

Figure 4: Image contrasts and seeing recorded at 19:02:39 UT, Sep 7, 2019

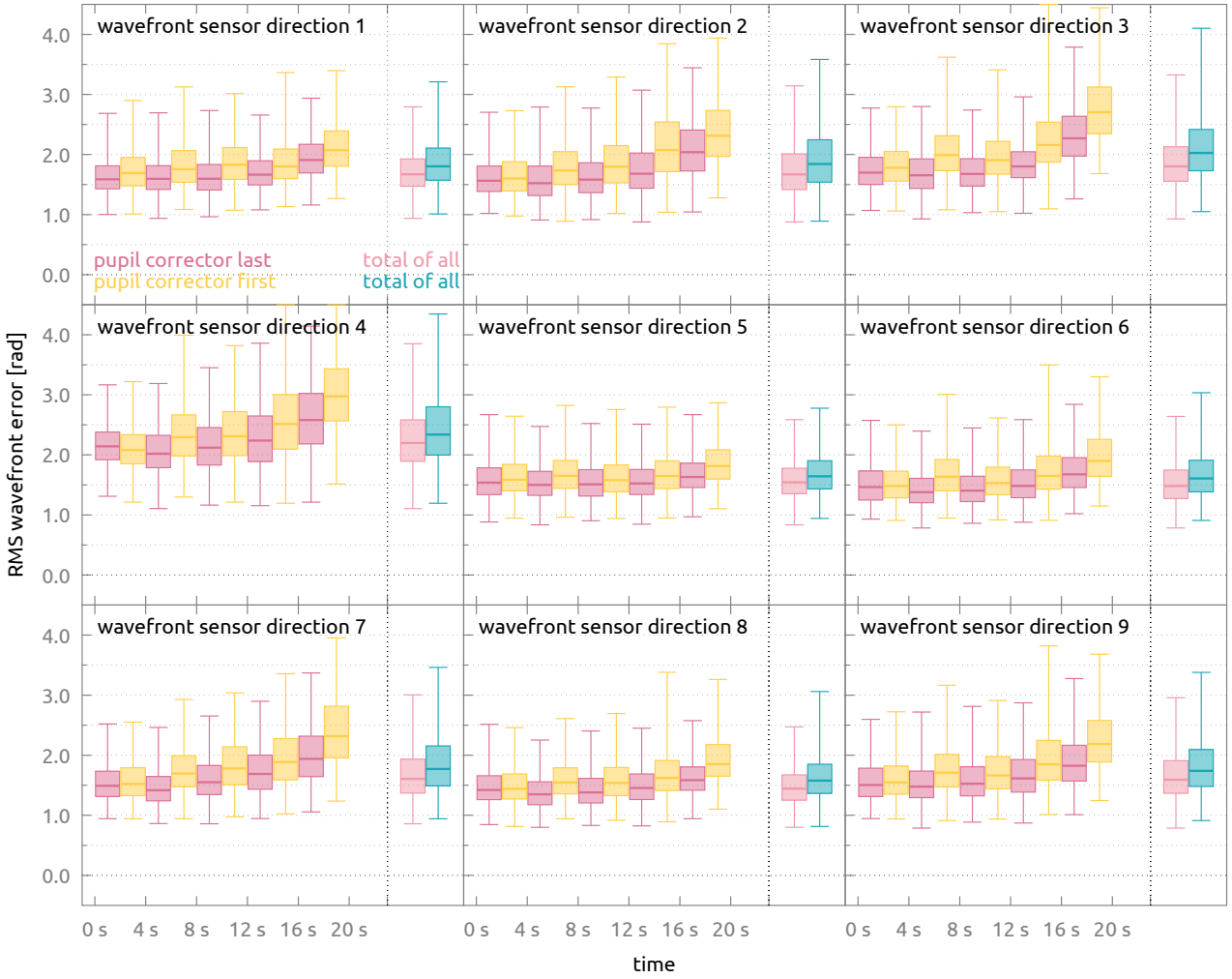

Figure 5: Residual wavefront errors recorded at 21:13:39 UT, Sep 6, 2019

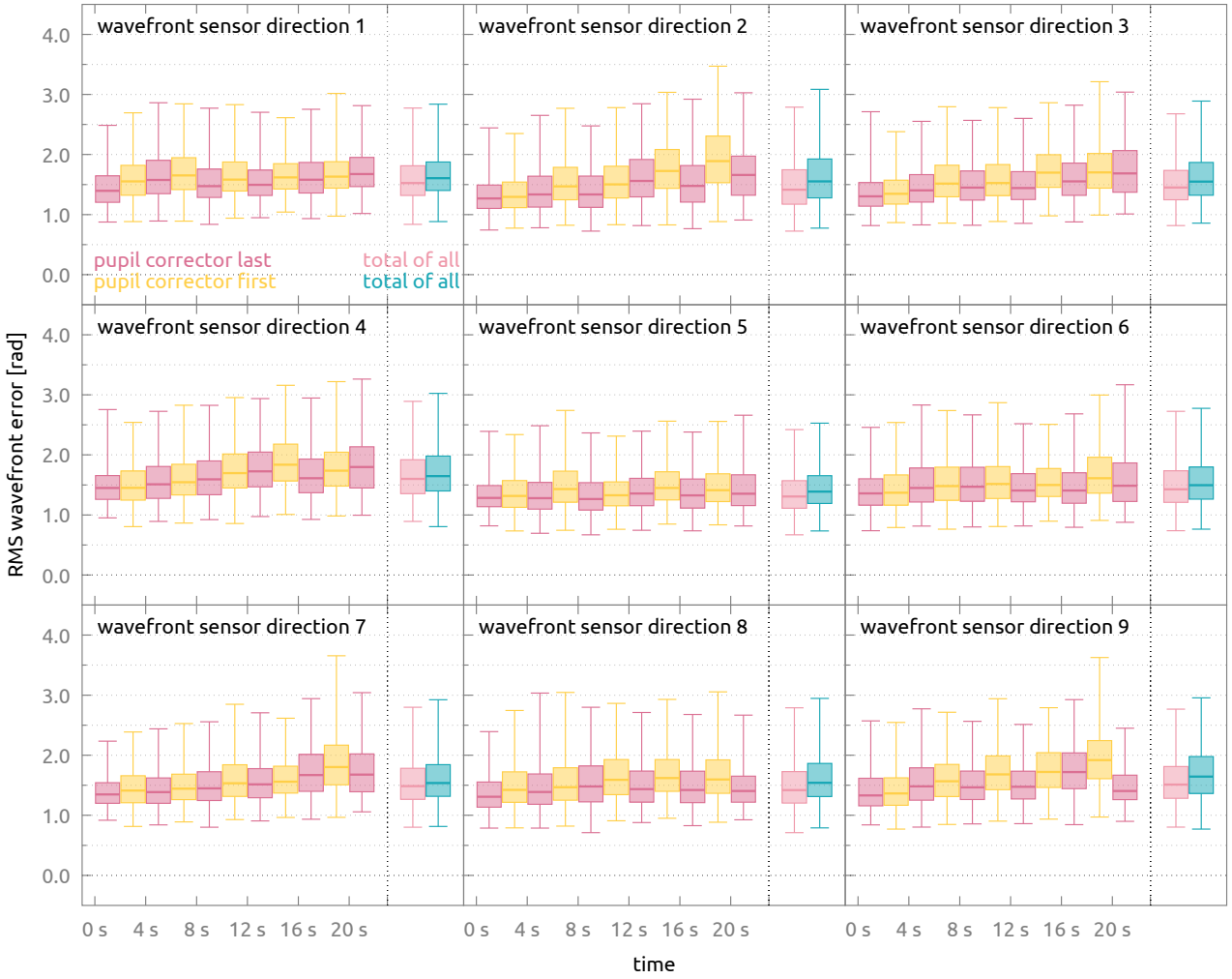

Figure 6: Residual wavefront errors recorded at 21:13:39 UT, Sep 6, 2019

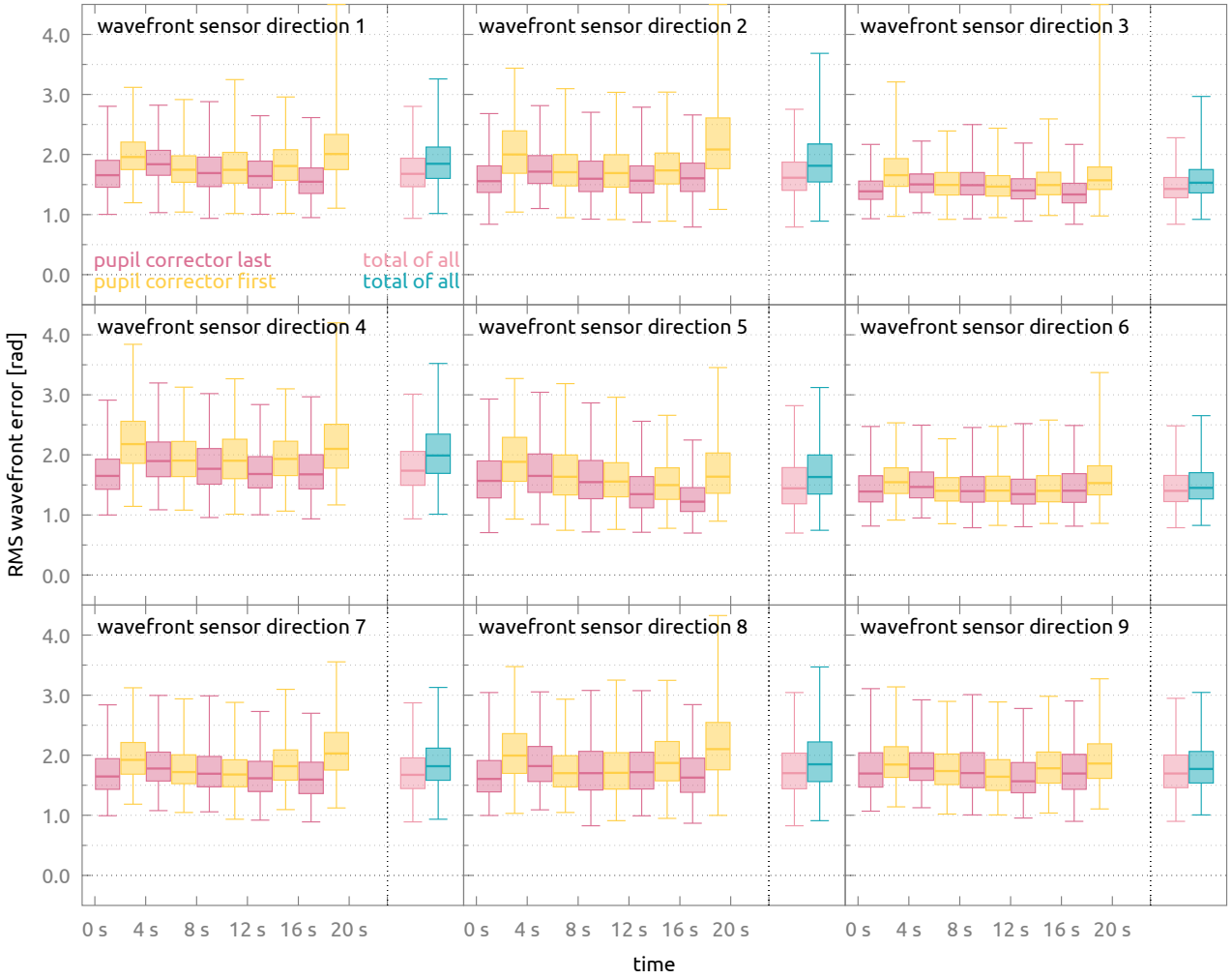

Figure 7: Residual wavefront errors recorded at 21:13:39 UT, Sep 6, 2019